Modeling the mid-infrared optical gap in $La_{2-x}Sr_xCuO_4$

F. Hanke and M. Azzouz*
Department of Physics and Astronomy, Laurentian University, 935 Ramsey Lake Road, Sudbury, Ontario, P3E 2C6 Canada

In this work, we used a periodic lattice potential in order to model the infrared optical data of the high-temperature superconductor $La_{2-x}Sr_xCuO_4$. This potential consists of a two-dimensional array of double-well potentials, which simulate the CuO_2 layers. It is obtained by assembling Cu-O-Cu units rather than Cu and O single atoms in the tight-binding approach. A gap separating two energy bands can be obtained and is used to fit the infrared (IR) optical gap of this cuprate. We derived the dielectric function and showed that in the classical limit it reduces to the one consisting of a Drude term plus a number of lorentz components, equivalent to the dielectric function used empirically by several authors in their fits of the reflectivity. By refitting available reflectance data, we deduced a simple law for the doping dependence of the optical gap in $La_{2-x}Sr_xCuO_4$. In the present study, we argue that the optical gap is distinct from the pseudogap or the two-magnon gap, because it characterizes $La_{2-x}Sr_xCuO_4$ for all doping regimes.

PACS numbers: 74.25.Gz, 74.25.Jb, 74.25.Fy

I. INTRODUCTION

The optical properties of high-temperature superconductors (HTSC's) were examined shortly after the discovery of their superconductivity in order to understand the electronic structure of these materials. In the absence of a well-established theory of HTSC's, several authors have fitted their data using a dielectric function consisting of two terms, which correspond to the Drude contribution and at least one Lorentz oscillator component. [1–5] In some other reports, the optical conductivity was analyzed using the extended Drude theory.[6–8] In the former approach at least one contribution from an optical gap in the IR region is used. Many experimentalists have confirmed that this gap has energies in the range of 0.5 to 1 eV. However, to the best of our knowledge, the origin of the oscillator contribution has not yet been elucidated. In this paper we propose a model for the origin of this gap. Using the peculiar crystal structure of HTSC's, which is characterized by CuO_2 layers, we propose a two-dimensional periodic lattice potential to be at the origin of this gap. While we focus our analysis on $La_{2-x}Sr_xCuO_4$ because optical data are available for all doping regimes for this material, we think that the present approach could apply to all those HTSC's with a similar optical gap.

Two gaps possibly exist in HTSC's, but neither of these is suitable for accounting for the gap found in the IR region. First, the spin fluctuations are believed to give rise to a *gap* in the range 0.1 to 0.15 eV. Second, the separation between the oxygen and copper bands is believed to yield a gap of about 2 eV in the vicinity of half filling. Uchida *et al.*[2] have discussed the origin of the IR optical features in $La_{2-x}Sr_xCuO_4$ and concluded that the results are similar to those predicted from the t-J model. However, in the t-J model, they noted, $J \sim 0.1$ eV cannot lead to a gap higher than 0.1 eV or so. Furthermore, the optical gap is observed well above the pseudogap temperature near the optimal doping density in $La_{2-x}Sr_xCuO_4$. This may be taken as an argument that the optical gap is much less sensitive to the electronic correlations than the pseudogap, for example. Therefore for the sake of simplicity we focus our analysis on room temperature data in order to obtain a model for the optical gap. We assume that the optical gap is due to a periodic crystal potential.

This paper is organized as follows. First, we give a detailed description of the double-well potential (DWP) model in Sec. II, then describe its optical properties quantum mechanically in Sec. III. Next, we discuss the fitting of the IR reflectance data by using the usual classical models and redo some of the fits, which were done by other researchers, in Sec. IV. We discuss our results in Sec. V, and conclude this work in Sec. VI.

II. EFFECTIVE POTENTIAL FOR THE COPPER-OXIDE LAYERS

There is significant experimental evidence according to which the hybridization of the O 2p and Cu 3d orbitals plays an important role in the electronic structure of HTSC's.[2, 9, 10] Here, we modeled such an overlap of orbitals by considering a potential with minima situated between the oxygen and copper atoms. According to that experimental evidence, these potential minima should be closer to the oxygen atom than the copper atom. The idea consisted of viewing HTSC's as materials synthesized by assembling copper-oxygen-copper units to form the CuO_2 layers, which are thought to dominate the low energy physics. We then modeled the copper-oxygen-copper edges of a CuO_2 unit cell in a CuO_2 layer using a simplified electronic DWP, whose parameters are chosen so that there are exactly two stationary states inside any DWP when the DWP's are far apart from each

*Electronic address: mazzouz@laurentian.ca

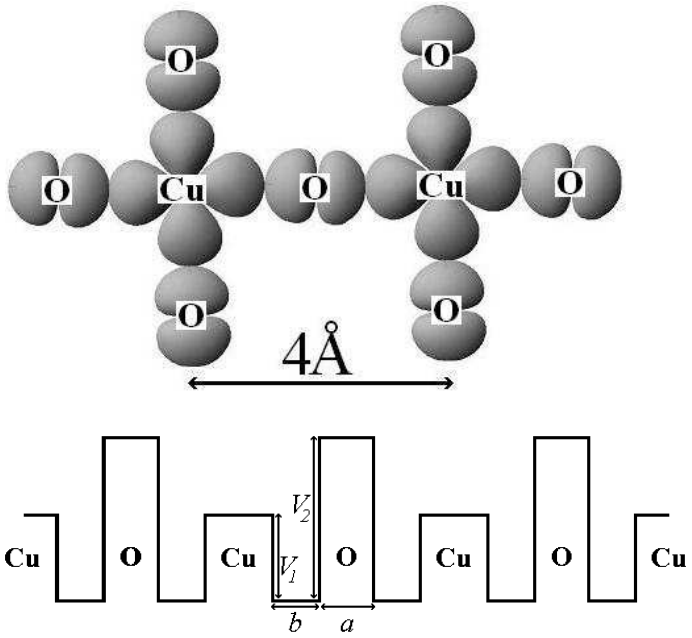

FIG. 1: (top) The electronic states in the CuO_2 plane that are thought to play the major role in the low-energy properties of the cuprates are based on the Cu $d_{x^2-y^2}$ and O p_σ orbitals. (bottom) The DWP is shown for three unit cells along either $\hat{\mathbf{a}}$ or $\hat{\mathbf{b}}$ crystal axis. The spatial dimensions of the well are a=0.66 Å and b=1.34 Å. The Cu-Cu distance is taken to be ≈ 4 Å.

other. The difference between their energy levels yields a gap in the IR range. We should mention that the idea of modeling the electronic structure using the O 2p orbitals and Cu 3d orbitals goes back to the earlier days of HTSC's.[11]

Figure 1 shows the effective DWP that has been used in order to represent the Cu-O-Cu structure along either the $\hat{\mathbf{a}}$ or $\hat{\mathbf{b}}$ axis. This figure also shows the atomic orbitals of the Cu and O atoms involved in the overlap. It is these DWP's that are assembled in order to form the CuO_2 layers but not the single oxygen and copper atoms. The tight-binding method is used to describe the assembly process. Within this model, we derived quantum mechanically the expression for the dielectric function that has been used in the empirical fits of various optical data. Our model is meant to fit room temperature optical data near optimal doping or optical data above the pseudogap temperature T^* for all doping levels. In order to extend the present treatment to lower temperatures, one would have to include electron interactions. Above T^* or away from half-filling, we expect Coulomb repulsion to play a much less relevant role than at lower temperatures and near half filling. Because T^* is most likely a consequence of electron correlations and the optical gap is observed[12] even above T^* the approximation of neglecting the electronic interactions in the present approach is justified. In addition, the almost accepted viewpoint that HTSC's can be described by a two-dimensional hubbard-like model at low energies is not in collision with the picture that we draw here.

We are interested in the energy eigenvalues below the lower barrier V_1. We first solve the Schrödinger equation for a single DWP, then later on we will assemble an infinite array of DWP's using the tight-binding approach. We define the dimensionless quantities

$$\tilde{V}_i = \frac{V_i}{E_0}, \tag{1}$$

where $E_0 = \hbar^2/(2m_e b^2)$, with $i = 1$ or 2, and m_e is electron's mass. Starting from the Schrödinger equation for the Hamiltonian of a single DWP, the energy eigenvalues E can be found by solving the following transcendental equations

$$\tan\sqrt{\tilde{E}} = \frac{\sqrt{\tilde{E}(\tilde{V}_1-\tilde{E})}+\sqrt{\tilde{E}(\tilde{V}_2-\tilde{E})}\tanh(\frac{a\sqrt{\tilde{V}_2-\tilde{E}}}{2b})}{\tilde{E}-\sqrt{(\tilde{V}_2-\tilde{E})(\tilde{V}_1-\tilde{E})}\tanh(\frac{a\sqrt{\tilde{V}_2-\tilde{E}}}{2b})} \tag{2}$$

for even wave functions, and

$$\tan\sqrt{\tilde{E}} = \frac{\sqrt{\tilde{E}(\tilde{V}_1-\tilde{E})}\tanh(\frac{a\sqrt{\tilde{V}_2-\tilde{E}}}{2b})+\sqrt{\tilde{E}(\tilde{V}_2-\tilde{E})}}{\tilde{E}\tanh(\frac{a\sqrt{\tilde{V}_2-\tilde{E}}}{2b})-\sqrt{(\tilde{V}_2-\tilde{E})(\tilde{V}_1-\tilde{E})}} \tag{3}$$

for odd wave functions. Here $\tilde{E} = E/E_0$, and $a = 0.66$ Å and $b = 1.34$ Å, giving $E_0 = 2.12$ eV. We choose the parameters $\tilde{V}_1$ and $\tilde{V}_2$ so that there are two energy levels below the smallest barrier V_1. The difference between these two energy levels is proposed to be at the origin of the IR gap in $La_{2-x}Sr_xCuO_4$ and perhaps in other HTSC's with an optical gap. For $V_1 = 8.5$ eV and $V_2 = 17$ eV, figure 2(a) displays the wavefunctions $\psi_{GS}(x)$ and $\psi_{EX}(x)$ of

the ground and excited states, respectively. The ground-state and excited-state energies are $E_1 = 2.16E_0 = 4.57$ eV and $E_2 = 2.99E_0 = 6.34$ eV, respectively. For a one-dimensional array of DWP's, we calculated the dispersion of the energy levels by using the tight-binding method. The essence of this method here consists of bringing together the Cu-O-Cu units from infinity. This consists of using the stationary states of our DWP's in lieu of the atomic orbital basis in order to obtain a band structure. The latter is shown in figure 2(b) for the one-dimensional periodic potential obtained by assembling the unit potentials displayed in figure 2(a). The important feature of this structure is that there always exists a finite energy gap between the two bands, which is used to fit the IR gap. To leading order, to get a two-dimensional array we combine sets of DWP's along the $\hat{\mathbf{a}}$ and $\hat{\mathbf{b}}$ axes together, and use that to model the CuO_2 layers in HTSC's. We expect that this approach is a good approximation because the overlaps of the wavefunctions $\pi/4$ from $\hat{\mathbf{a}}$ or $\hat{\mathbf{b}}$ are much smaller in real materials. Note that the wavefunctions in Fig. 2(a) are consistent with the fact that in the hybridized state, it is more likely to find the electron near the oxygen atom. This is given here by a higher probability density near the oxygen atom.

For a given doping density, we need to figure out the filling of the bands. The number of available wavevectors is equal to the number of copper sites, N, within a given CuO_2 plane. Every available state can accommodate at most two electrons due to the Pauli exclusion principle. In an undoped copper-oxygen plane, there is exactly one electron per copper site. In the ground state, only the lowest band is exactly half-filled at zero doping, while doping consists of adding to or removing electrons from the lower band. Note that this analysis is consistent with the tight-binding band in the single-band Hubbard-type models often used to study HTSC's. For energies roughly smaller than 0.1 eV, only the lower band in Fig. 2 will contribute. For higher energies, one expects that the higher band would start contributing regardless of whether on-site Coulomb repulsion U is included or not. As far as charge dynamics is concerned Coulomb repulsion would split the lower DWP band into two Hubbard bands separated by an energy of the order of U. However, the separation between the lower Hubbard band and the higher DWP band would show in the optical properties before the separation between the lower and upper Hubbard bands does. So the present treatment would remain qualitatively correct even if U is included. The lower DWP band is pretty flat when compared to bands in ordinary metals. So, even though the lower band is half filled or less, thermally excited electrons would quickly reach the top of the lower band, and become available for optical transitions in the case of s.

III. THE DIELECTRIC FUNCTION OF THE DWP'S

In order to calculate the dielectric response of the two-dimensional array of the DWP's, we need to know the electron density $n(\mathbf{q}, t)$ within the DWP lattice caused by an AC electric field $\mathbf{E}$. The polarization density $\mathbf{P}$ can be calculated via

$$\nabla \cdot \mathbf{P} = -en(\mathbf{q}, t), \tag{4}$$

where e is electron's charge. $\mathbf{P}$ is related to the dielectric function by

$$\mathbf{P}(\mathbf{q}, t) = \frac{1}{4\pi}[\varepsilon(\omega, \mathbf{q}) - \varepsilon_\infty]\mathbf{E}(\mathbf{q}, t), \tag{5}$$

where $\varepsilon(\omega, \mathbf{q})$ is the dielectric function, and ε_∞ is its integrated contribution for very high frequencies. $\mathbf{q}$ is the momentum transfer from the reflected light to an electron within the DWP layer.

The induced electron density is calculated by applying a time-dependent perturbing potential to the system of DWP's. If we denote the electron wavevector $\mathbf{k}$ and the band index $\nu = 1$ or 2 with $\ell = \{\mathbf{k}, \nu\}$, the elements of the first order correction $\rho^{(1)}$ to the unperturbed system's density matrix will be given by [13, 14]

$$\langle \ell | \rho^{(1)} | \ell' \rangle = \frac{f(E_{\ell'}) - f(E_\ell)}{E_{\ell'} - E_\ell - \hbar\omega - i\hbar\alpha} \langle \ell | V(\mathbf{r}, t) | \ell' \rangle, \tag{6}$$

where $V(\mathbf{r}, t)$ is the potential of the incident light. Now the actual electron density can be calculated from the operator[15] $n = \sum_{\mathbf{r}_e} \delta(\mathbf{r}_e - \mathbf{r})$ with the summation taken over all possible electronic positions $\mathbf{r}_e$. The result is written in terms of the matrix elements $(\mathbf{k}, \nu | \mathbf{k} + \mathbf{q}, \nu') = \langle \mathbf{k}, \nu | e^{-i\mathbf{q}\cdot\mathbf{r}} | \mathbf{k}+\mathbf{q}, \nu' \rangle$ and the Fourier transform $V(\mathbf{q}, t) = \int d\mathbf{r} V(\mathbf{r}, t) e^{-i\mathbf{q}\cdot\mathbf{r}}/(2\pi)^2$ of $V(\mathbf{r}, t)$, and is given by

$$\langle n(\mathbf{q}, t) \rangle = \sum_{\nu,\nu'} \int \frac{d\mathbf{k}}{(2\pi)^2} \mid (\mathbf{k}, \nu | \mathbf{k} + \mathbf{q}, \nu') \mid^2 \frac{f(E_{\mathbf{k},\nu}) - f(E_{\mathbf{k}+\mathbf{q},\nu'})}{E_{\mathbf{k},\nu} - E_{\mathbf{k}+\mathbf{q},\nu'} - \hbar\omega - i\hbar\alpha} V(\mathbf{q}, t), \tag{7}$$

which yields the quantum mechanical expression for the dielectric function

$$\varepsilon(\omega, \mathbf{q}) = \varepsilon_\infty - \lim_{\alpha \to 0} v_q \int \frac{d\mathbf{k}}{(2\pi)^2} \sum_{\nu,\nu'} \mid (\mathbf{k}, \nu | \mathbf{k} + \mathbf{q}, \nu') \mid^2 \frac{f(E_{\mathbf{k},\nu}) - f(E_{\mathbf{k}+\mathbf{q},\nu'})}{E_{\mathbf{k},\nu} - E_{\mathbf{k}+\mathbf{q},\nu'} - \hbar\omega - i\hbar\alpha}. \tag{8}$$

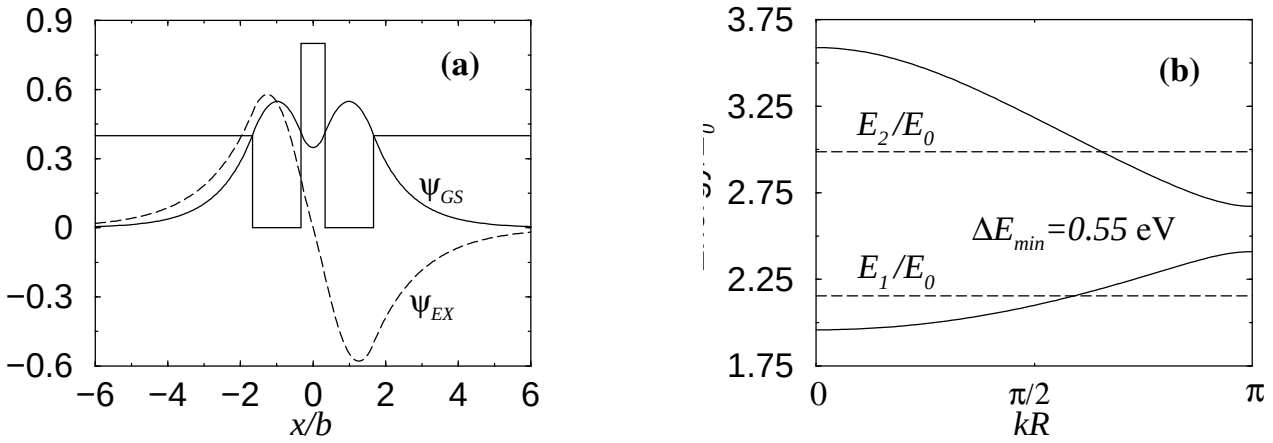

FIG. 2: (a) The ground and excited states for a DWP with $V_1 = 8.5$ eV and $V_2 = 17$ eV are shown versus x/b. (b) The energy bands that arise from a one-dimensional array of DWP's are displayed. The vertical energy axis in (b) is dimensionless as defined in equation (1). We note that the lowest band is 1/2 full at zero doping, as explained in the text. ΔE_{min} is the minimum of the energy difference between the two bands. E_1 and E_2 are the energies for the ground state ψ_{GS} and the excited state ψ_{EX}, respectively. Here $E_0 = 2.12$ eV and the calculation is illustrated for $R = 5$ Å.

Here, $v_q = 4\pi e^2/q^2$.

The classical limit of equation (8) consists of taking the limits $\alpha \to 0$ and $q \to 0$ and is valid for (flat) bands with low dispersion. The first limit has to be taken in the derivation of (6), where it is assumed that the perturbing potential is introduced infinitely slowly. The second limit comes from the fact that the norm of the momentum transfer $\mathbf{q}$ from a photon to an electron is two orders of magnitude smaller than the typical wavevectors of the Brillouin zone,[14] which means that $\mathbf{q}$ is essentially negligible in an integration over all $\mathbf{k}$'s. For this calculation, the summation in equation (8) has to be divided first into inter- and intraband contributions (which have $\nu = \nu'$ and $\nu \neq \nu'$, respectively), and then into real and imaginary parts. The terms $(\mathbf{k}, \nu|\mathbf{k}+\mathbf{q}, \nu')$ are evaluated using perturbation theory,[16] where the first order term involving the momentum operator for q in the Hamiltonian is the perturbation. The result essentially takes on the form

$$\varepsilon(\omega) = \varepsilon_\infty + \frac{\omega_{gp}^2}{\omega_G^2 - \omega^2 - i\omega\gamma_G} - \frac{\omega_{dp}^2}{\omega(\omega + i\gamma_d)}, \quad (9)$$

which corresponds to a Drude term plus a Lorentz oscillator contribution. Note that expression (9) can also be derived by writing down Newton's second law for conduction and bound electrons in a solid, and calculating the dielectric function.[17] The Lorentz oscillator term is the contribution from the bound charges. This contribution can be calculated for charges bound to *specific molecules* in a material by saying that the electrons are attached to the end of imaginary springs with force constant $-m\omega_G^2 x$. One then can solve Newton's second law with the total force given by $-m\gamma_G dx/dt - m\omega_G^2 x - eE_0\cos(\omega t) = md^2x/dt^2$ where $E_0\cos(\omega t)$ is some external electric field, and $-m\gamma_G dx/dt$ is some damping force.

The parameters commonly used for the empirical model (9) are the plasma frequencies ω_{dp} and ω_{gp}, the gap frequency ω_G, and the inverses of the Drude and oscillator relaxation times, γ_D and γ_G, respectively. In the present work these parameters are used as doping dependent fitting parameters. Equation (9) will be used in the next section in the fitting of some experimental data. The main difference between (9) and the actual limit in Eq. (8) is that the limit includes an integration over ω_G in the Lorentz oscillator, which comes from the $\mathbf{k}$ dependence of the energy difference $\hbar\omega_G = E_{\mathbf{k},\nu'} - E_{\mathbf{k},\nu}$. Our classical model utilizes only a single gap frequency, but several experimentalists have modeled their data using more than one energy gap,[1, 5] with the dielectric function given by

$$\varepsilon(\omega) = 1 - \frac{\omega_{dp}^2}{\omega(\omega + i\gamma_d)} + \sum_i \frac{\omega_{ip}^2}{\omega_i^2 - \omega^2 - i\gamma_i\omega}. \quad (10)$$

In Eq. (10), the summation $\sum_i$ takes now several oscillator contributions into account. In general, the energies of the different oscillators are very close to each other. We can interpret this summation as resulting from replacing the interband integral in equation (8) by a finite number of terms.

IV. REFLECTIVITY DATA FITTING

A. Doping dependence of the optical gap

The dielectric function given in equation (9) was used to fit the reflectance data of $La_{2-x}Sr_xCuO_4$. The re-

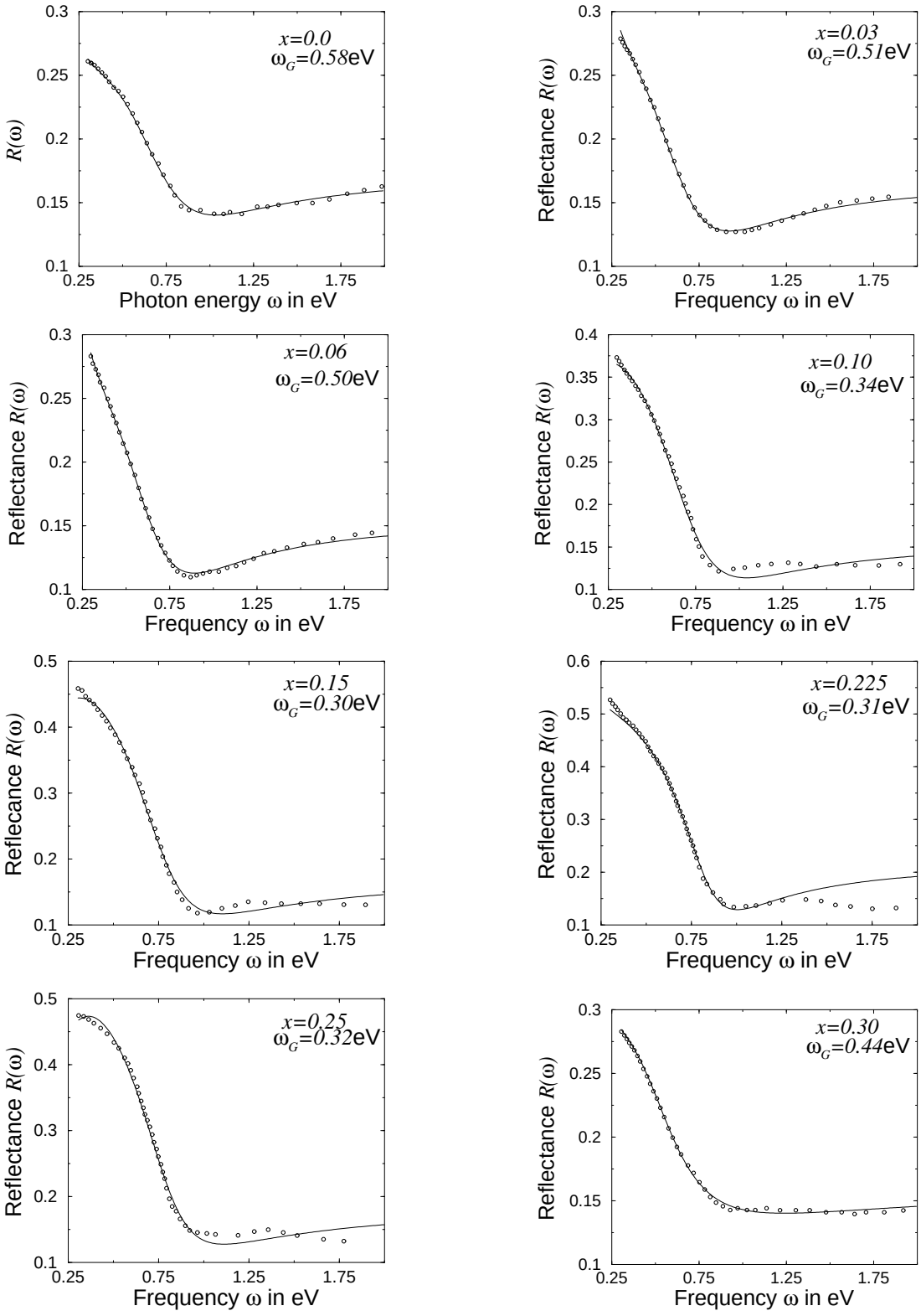

FIG. 3: The fits for the reflectance based on the dielectric function (9) for eight different compositions of polycrystalline $La_{2-x}Sr_xCuO_4$. The experimental data are taken from Ref. [[4]]. Shown on the figures are the doping constant x for each sample and the Lorentz gap frequency ω_G.

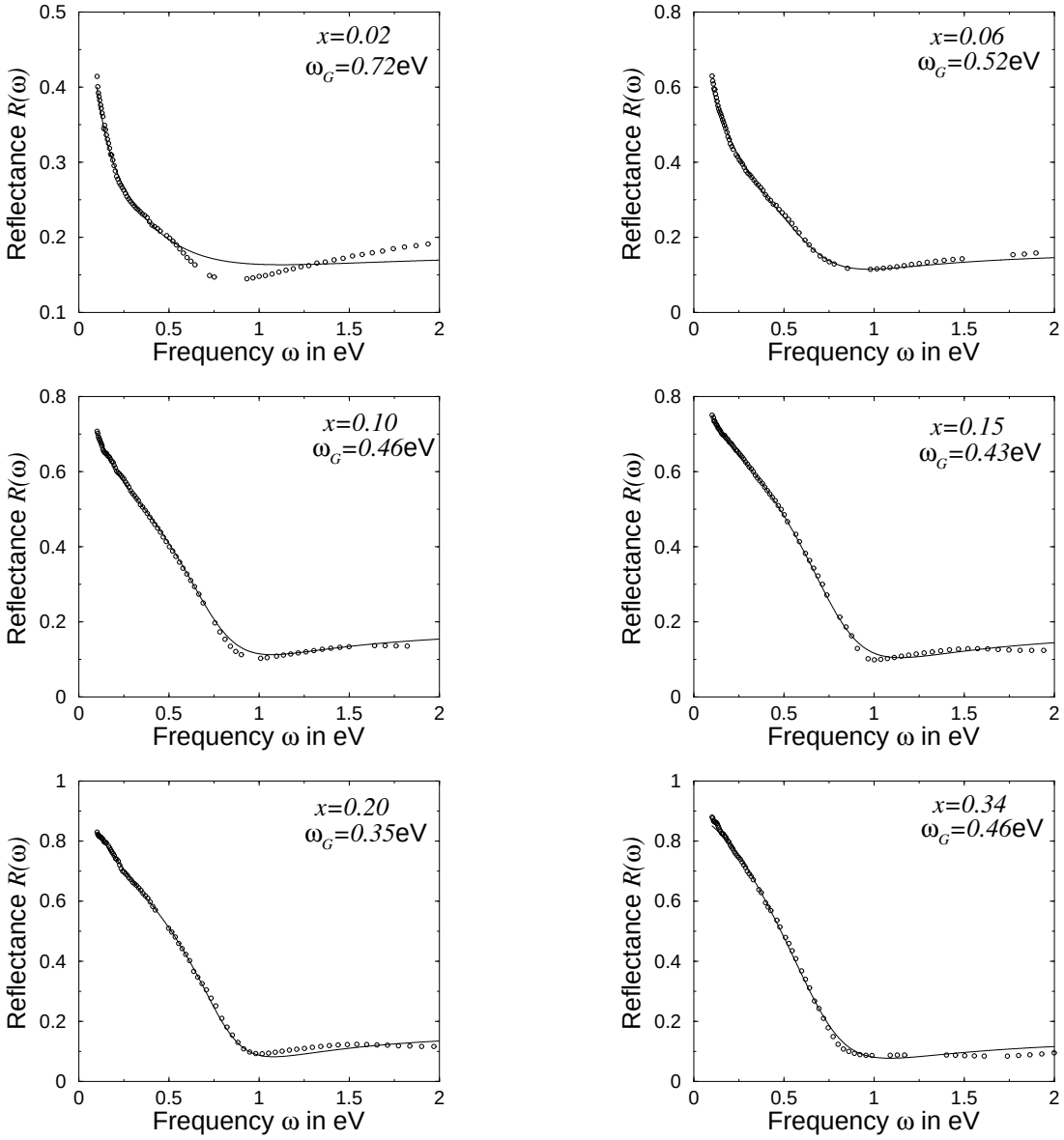

FIG. 4: Fits for the in-plane reflectance of single crystals of $La_{2-x}Sr_xCuO_4$. The data are taken from Ref. [[2]].

flectance is given by

$$R = \frac{1 - \sqrt{2(\sqrt{\varepsilon_1^2 + \varepsilon_2^2} + \varepsilon_1)} + \sqrt{\varepsilon_1^2 + \varepsilon_2^2}}{1 + \sqrt{2(\sqrt{\varepsilon_1^2 + \varepsilon_2^2} + \varepsilon_1)} + \sqrt{\varepsilon_1^2 + \varepsilon_2^2}}, \qquad (11)$$

where ε_1 and ε_2 are the real and imaginary parts of the dielectric function, respectively.

We have refitted $La_{2-x}Sr_xCuO_4$ reflectance data which were measured at room temperature by two groups of researchers. The results are displayed in figures 3 and 4. These plots have been obtained by minimizing the sum of least squares using a Monte Carlo method. In table I we show the parameters used for the best fits which generally have an accuracy of 99% or so. Note that there are some differences in the spectra for single and polycrystalline materials. For the polycrystalline material, following Etemad *et al.*, [4] we have scaled the results of the reflectance we calculated by 2/3 in order to simulate the reduction in R due to polycrystallinity.[3]

For the polycrystalline samples, the fits in figure 3 are good for doping $x = 0$, 0.03, 0.06 and 0.30. For $x = 0.1$, 0.15, 0.225, and 0.25 the fits are less accurate. Comparison shows that the fits in Fig. 3 for the polycrystalline samples are less accurate than those in Fig. 4 for the single crystals. This difference is perhaps due to polycrystallinity which introduces a higher energy contribution; in figure 4, we note that except for $x = 0.02$ the fits are excellent for all other doping concentrations. For the data of Fig. 3, the c-axis of the $La_{2-x}Sr_xCuO_4$ crystals was randomly oriented with respect to the light po-

larization because of the polycrystalline character of the sample. For the data fitted in Fig. 4, the light was polarized perpendicular to the c-axis,[2] which means that this experiment probed essentially those electrons moving in the CuO_2 planes.

One of the important results we obtained is the doping dependence shown by the energy gap ω_G of the numerical fits. ω_G is given in table I. As illustrated in figure 5, we found that ω_G is well fitted by a parabolic dependence on doping

$$\omega_G = A(x - B)^2 + C$$

for both the single crystal and polycrystalline material. ω_G shows a minimum for both data not far from optimal doping. In the absence of a clear understanding of the origin of this minimum, one can speculate that it perhaps is a consequence of the electronic structure reconstruction taking place as doping increases.[2] We cannot explain its presence in terms of only bound charges performing transitions from the lower band to the upper band with no other effects contributing. Otherwise said, the doping dependence of the gap ω_G would imply that the two bands or the DWP's evolve as a function of doping. Note also that we cannot claim that this minimum is a universal property of all HTSC's. One has to examine the data for other high-T_C materials in order to reach a conclusion about the universality of the existence of this minimum.

Table I shows the values of all the fitting parameters of Eq. (9) for both the poly- and single crystals. For comparison, table II gives the values of ω_G and γ_G used in the fits of experimental data by two other research groups for $La_{1.825}Sr_{0.175}CuO_4$, $Bi_2Sr_2CaCu_2O_8$, and $YBa_2Cu_3O_{6.9}$.[1, 3] These values are comparable to those we report in table I.

B. Doping dependence of the plasma frequencies

While the doping dependence of ω_G shows this parabolic behavior the doping dependence of the other parameters listed in Table I cannot be easily fitted. However the plasma frequencies do show some clear tendencies. Etemad *et al.*[4] defined the plasma frequency ω_p by writing $\omega_{gp}^2 = \omega_p^2 f_G$ and $\omega_{dp}^2 = (1 - f_G)\omega_p^2$ where f_G is the fraction of the total electronic oscillator strength consumed in the optically allowed transition across the gap. Therefore $\omega_p^2 = \omega_{dp}^2 + \omega_{gp}^2$. One can write $\omega_p^2 = 4\pi n_t e^2/m^*$ where m^* is an effective mass of the charge carrier, e the electron charge, and n_t the sum of the free and bound charge densities. In Figure 6(a), we plot $\omega_p^2(x)$ extracted from table I versus x. For the single crystals data of Uchida *et al.*, the doping dependence of ω_p^2 clearly reflects on the fact that the charge carrier density increases as doping x increases away from half-filling, but ω_p^2 reaches a maximum near optimal doping, then slightly decreases in the overdoped regime. For the polycrystalline samples, the same general behavior is observed except near half-filling, where ω_p^2 decreases slightly before increasing linearly for $0.06 \leq x \leq 0.15$, and reaching a maximum rather away from the optimal point at $x = 0.25$. The significant difference between the two sets of data can be attributed to the spatial anisotropy in the polycrystalline samples. Of course, the data of the polycrystalline samples are less reliable than those of the single crystals. Note that Orenstein *et al.* reported that $\omega_p \approx 2$ eV yields $n \sim x$ (in cm^{-3}) if $m^*/m = 0.8$. For Uchida *et al.*'s data we find $\omega_p \sim 2$ eV near the optimal point. The finite value of ω_p^2 at $x = 0$ can perhaps be attributed in part to the fact that the oxygen content is not exactly 4 in $La_{2-x}Sr_xCuO_4$. Also, because of the strong temperature dependence of the Hall coefficient, thus of the Hall density, one would not expect to find ω_p^2 behaving simply linearly with x.[18–20] Note however that a linear fit for $0.06 \leq x \leq 0.15$ extrapolates almost to 0 for both sets of data. Overall, the doping dependence of ω_p^2 shows a trend qualitatively consistent with doping. It is equally important to find that the doping dependence of ω_p^2 bears some resemblance to that of the superconducting transition temperature T_C (i.e., dome shape). Uemura *et al.*[21] found that T_C increases linearly with n_s/m^* as doping increases away from half-filling (n_s is the superconducting carrier density), saturates and then decreases in the heavily overdoped regime. This behavior is similar to the one we found here for ω_p^2.

In Figure 6(b), we plot ω_{dp}^2 and ω_{gp}^2 as a function of doping. The quantities ω_{dp}^2 and ω_{gp}^2 may be thought of as being proportional to the densities of the free and bound charge carriers, respectively. ω_{dp}^2 increases in the underdoped regime, passes through a maximum near optimal doping, and seems to saturate in the overdoped regime. The bound charges density seems to undergo a sudden jump near optimal doping. This density seems to be roughly constant in the underdoped and overdoped regimes. Again these features are perhaps a consequence of the electronic structure reconstruction taking place as doping evolves. These results are consistent with a change from hole-like to electron-like charge carriers taking place in the overdoped regime in $La_{2-x}Sr_xCuO_4$ because the charge carrier density does not keep increasing with doping beyond the optimal point.[22]

C. Doping dependence of the scattering rates

We will discuss only the scattering rates for the single crystals data of Uchida *et al.*'s. Figures 7(a) and 7(b) display the Drude and oscillator scattering rates γ_d and γ_g plotted versus doping. The Drude rate γ_d shows a clear doping dependence trend for γ_d overall decreases by an order of magnitude when we go from the underdoped to the overdoped regime. The mean-free path $\ell_d = v_0/\gamma_d$ can be estimated using a speed $v_0 \sim 10^5$ m/s (obtained from $mv_0^2/2 \sim k_B T$). One finds $\ell_d \sim 1$ to 10 Å for $\gamma_d \sim 1$ to 0.1 eV. This means that the mean-free path is of the order of the lattice spacing parameter (Cu-Cu distance) deep in the underdoped regime, but

TABLE I: The parameters used in the reflectance fits of figures 3 and 4 are summarized in this table. The frequencies, γ_d, and γ_G are given in eV. The data for polycrystalline samples are shown in the upper panel, and for single crystals in the lower one.

Reference	x	ϵ_∞	ω_G	ω_{dp}^2	γ_d	ω_{gp}^2	γ_G
Etemad *et al.*[4]	0.0	9.37	0.58	1.26	0.45	2.46	0.72
	0.03	8.95	0.51	1.61	0.37	1.82	0.68
	0.06	8.10	0.50	1.84	0.41	1.22	0.61
	0.10	8.34	0.34	1.82	1.78	3.71	0.48
	0.15	9.30	0.30	4.23	1.65	4.39	0.32
	0.225	13.37	0.31	4.89	0.18	4.98	0.58
	0.25	10.31	0.32	5.99	1.88	4.94	0.25
	0.30	8.52	0.44	5.59	1.90	1.04	0.51
Uchida *et al.*[2]	0.02	6.13	0.72	1.11	0.94	1.01	1.72
	0.06	5.56	0.52	1.21	0.38	1.21	0.81
	0.10	6.21	0.46	3.02	0.48	1.12	0.80
	0.15	6.09	0.43	3.13	0.36	2.00	1.06
	0.20	5.71	0.35	1.97	0.13	2.54	0.75
	0.34	5.06	0.46	2.05	0.12	2.19	1.14

TABLE II: The values of the gap frequency ω_G and γ_G used by other authors in their fits for two different materials are shown. These values compare well to ours. Orenstein *et al.*'s $La_{1.825}Sr_{0.175}CuO_4$ sample was a ceramic powder pressed into pellet form. The $Bi_2Sr_2CaCu_2O_8$ samples of Quijada *et al.* were single-domain crystals.

Authors	Material	ω_G in eV	γ_G in eV
Quijada *et al.*[1]	$Bi_2Sr_2CaCu_2O_8$	0.56	0.98
Orenstein *et al.*[3]	$La_{1.875}Sr_{0.125}CuO_4$	0.45	0.9
	$YBa_2Cu_3O_{6.9}$	0.65	1.3

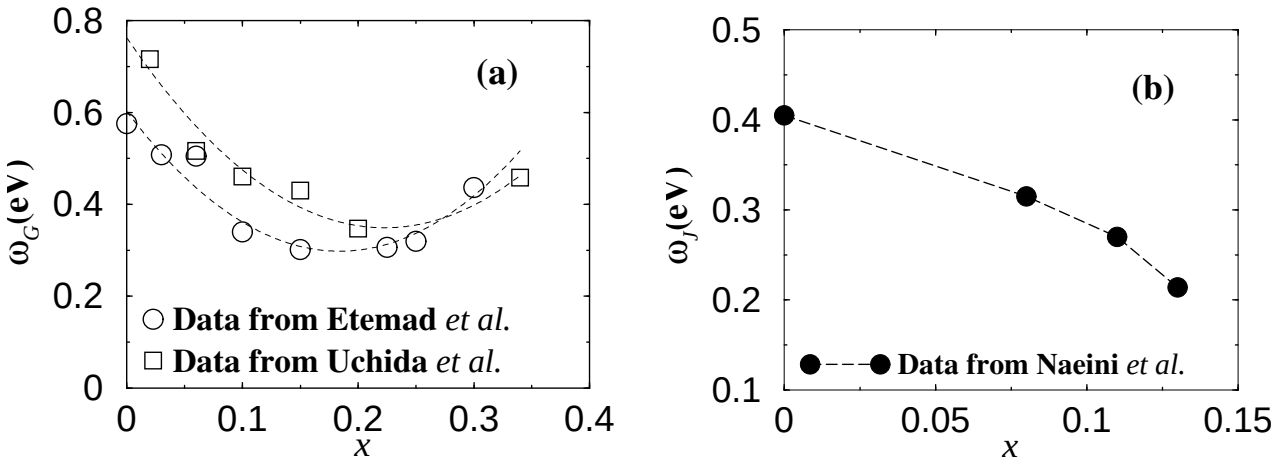

FIG. 5: (a) Parabolic fits for the doping dependence of the gap frequency are shown. The parameters for the fits for the data of Ref. [[4]] are $A = 8.979$ eV, $B = 0.184$, and $C = 0.298$ eV, while for the data of Ref. [[2]] we found $A = 8.314$ eV, $B = 0.223$, and $C = 0.349$ eV. Both of these parabolas have a sum of least squares less than or equal to 0.0001. Note that none of the other parameters of table I show an obvious dependence on doping. (b) For comparison, the x dependence of the two-magnon gap of $La_{2-x}Sr_xCuO_4$ taken from naeini et al.'s[26] paper is shown. The dashed line in (b) is a guide to the eye only.

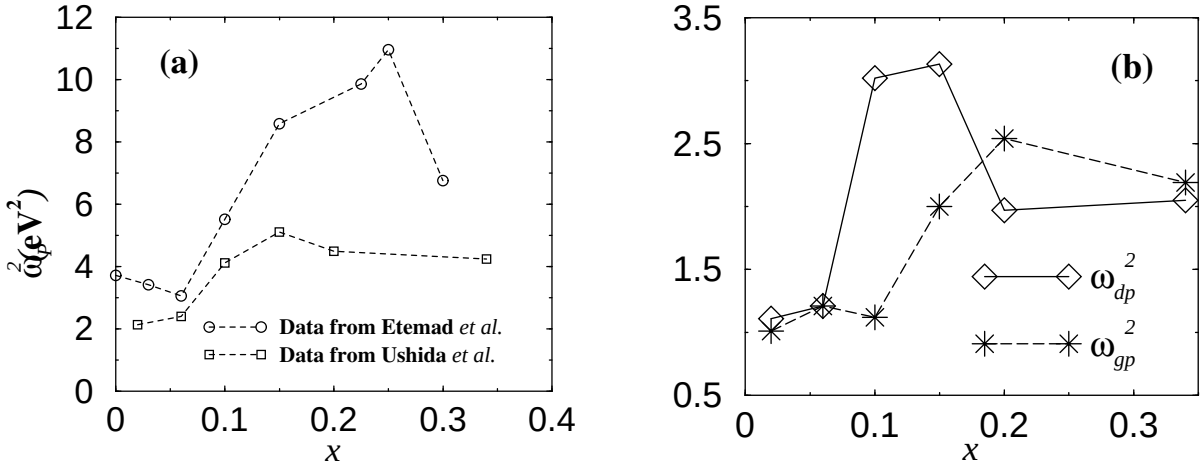

FIG. 6: (a) The doping dependence of ω_p^2 is displayed for both experimental data sets analyzed here. (b) That of ω_{dp}^2 and ω_{gp}^2 is displayed for Uchida *et al.*'s data only. The lines in (a) and (b) are a guide to the eye only.

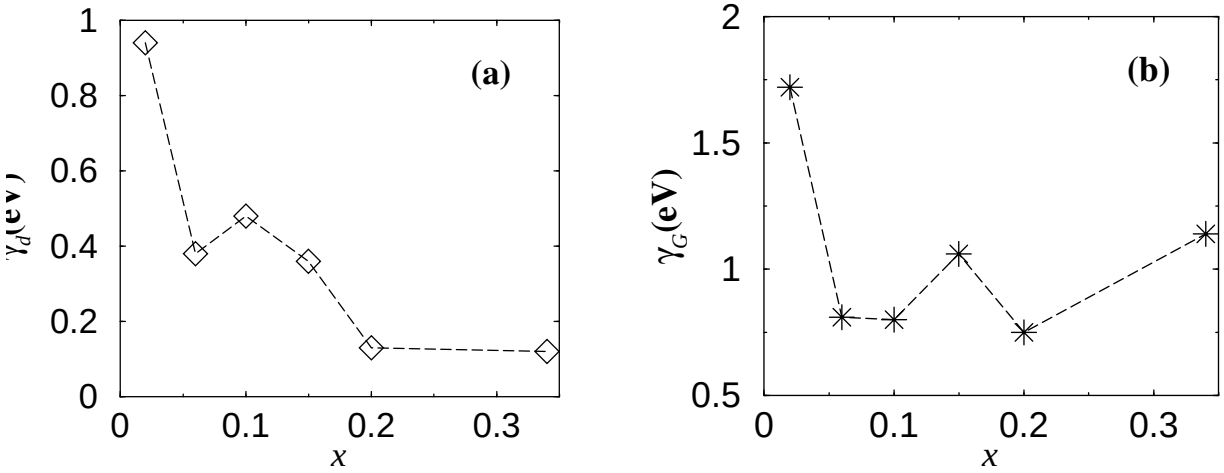

FIG. 7: The doping dependence of (a) γ_d and (b) γ_G is displayed for Uchida *et al.*'s data. The dashed lines are a guide to the eye only.

increases by an order of magnitude in the overdoped region. In HTSC's, inelastic scattering by bosons of some sort (probably spin fluctuations) dominates and gives rise to a scattering rate, which depends strongly on temperature, frequency and doping.[6] Note that in the present two-component model we did not consider the frequency dependence of γ_d and γ_G. Usually, this can be taken into account in the so-called one-component extended Drude model with only *free* type carriers with renormalized mass.[8] Here, the fact that γ_d or ℓ_d changes by an order of magnitude is consistent with the picture according to which the *free* type charge carriers are scattered by the antiferromagnetic spin fluctuations. As doping increases, these fluctuations diminish and vanish beyond a critical doping.[18, 19] Thus the saturation of γ_d above the optimal point in Fig. 7(a) can be explained by the fact that the spin fluctuations become irrelevant in the overdoped regime as far as scattering is concerned.

Concerning the oscillator contribution, one expects the rate γ_G not to show a strong dependence on doping. This is because γ_G is a contribution from electrons that move at most within a unit lattice cell across an energy gap. So the electron filling should not matter significantly. Except for doping 0.02, figure 7(b) shows that on average γ_G is not affected by doping. Using Uchida *et al.*'s data in table I we get the average of γ_G over doping $\langle\gamma_G\rangle = \sum_x \gamma_G(x)/N \approx 1.03$ eV, with $N = 6$ being the total number of doping densities. This average corresponds to an effective mean-free path of the order of the lattice parameter ($\ell_G \sim 1$ Å) in agreement with our explanation in terms of a localized damping.

V. DISCUSSION

In the phase diagram of HTSC's, a gap-like behavior takes place below a characteristic temperature T^* that decreases as doping increases and vanishes not far from the optimal doping.[23, 24] This feature was termed the pseudogap, because it appears in the normal state at temperatures much higher than the superconducting transition temperature T_C in the underdoped regime.[25] Roughly, the pseudogap E_g decreases as doping increases according to the simple law $E_g(x) \sim J(1 - x/0.3)$. The question of a possible connection between the pseudogap and the optical gap analyzed here has then to be addressed. Raman,[26] IR,[27] specific heat,[28] and angle-resolved-photoemission[29] experiments on $La_{2-x}Sr_xCuO_4$ all revealed that the pseudogap is of the order of $J \sim 0.1$ eV near half filling or smaller for higher doping. In figure 5(a), we see that the least of the minima of ω_G, which is 0.30 eV, is well above the pseudogap energy, especially in the vicinity of the optimal point. Also the dependence on doping of the two gaps is very different, as the pseudogap shows a more or less linear doping dependence in the underdoped regime. The gap in the optical properties shows little variation with temperature[1] and remains present well above room temperature even near optimal doping level. [2–4, 27] This leads us to conclude that the pseudogap and the optical gap have different origins. Note that Lupi *et al.*[12] studied the optical conductivity of $Bi_2Sr_2CuO_6$ with $T_C \approx 20$ K, and concluded that a multicomponent model for $\sigma(\omega)$ with the coexistence of free and bound charges is needed. In their work, a careful analysis led also to the conclusion that the optical gap is different from the pseudogap. These authors mentioned that the optical gap is observed in optical conductivity measurements even for temperatures greater than the pseudogap temperature T^*.

The IR optical gap is different from the two-magnon gap ω_J as well.[26, 30] The energies found for the optical gap in $La_{2-x}Sr_xCuO_4$ are higher than those found for the two-magnon excitation, and they have a roughly parabolic doping dependence as opposed to the roughly linear one found for the two-magnon gap. Also the two-magnon energy ceases to exist in the overdoped regime, and behaves as $\omega_J(x) \sim 3E_g(x)$ for $0 < x < 0.13$ in $La_{2-x}Sr_xCuO_4$.[26] For comparison, figure 5(b) shows the doping dependence of the two-magnon peak reported by Naeini *et al.*[26] for $La_{2-x}Sr_xCuO_4$. Clearly, this gap is much smaller than the optical gap and has a different doping dependence as can be seen in figures 5(a) and 5(b). Also for comparison, the two-magnon gap in $Bi_2Sr_2Ca_{1-x}Y_xCu_2O_{8+\delta}$ has a doping dependence that is very similar to that of $La_{2-x}Sr_xCuO_4$.[30] It looks then that three different energy gaps or pseudogaps characterize the normal state of HTSC's: the pseudogap in the underdoped regime, the optical gap, which is observed even in the overdoped regime, and the two-magnon gap, which is observed in the underdoped regime only. We believe that the pseudogap like the two-magnon gap is a consequence of antiferromagnetic correlations.[25] However, what we propose here is that the optical gap is a result of the periodic lattice potential.

As noted in Ref. [31] $La_{2-x}Sr_xCuO_4$ constitutes the extreme exception to the simple picture of the crossing of T^* and T_C scales at optimal doping. In most other families of HTSC's, T^* and T_C seem to become equal very close to optimal doping.[32] For $La_{2-x}Sr_xCuO_4$, Batlogg *et al.*[33] suggested that T^* remains significant even in the overdoped regime. These authors found that T^* becomes doping independent for doping level above the optimal point. This is pretty striking since there is no physical reason for the sudden leveling off of T^* for doping densities above the optimal point. We believe that the pseudogap is caused by antiferromagnetic correlations of some sort. One of the present authors proposed that rotating antiferromagnetism is responsible for the pseudogap.[18, 19] Naturally, one would think that these antiferromagnetic correlations would monotonously decrease as doping increases with no reason for saturation. The data of Startseva *et al.*[31] seem to indicate that the *gap* extracted form the optical data for $La_{2-x}Sr_xCuO_4$ is almost the same for $x = 0.184$ and $x = 0.22$. We thus think that what Startseva *et al.* measured in these overdoped samples is likely a gap that is not related to the pseudogap. This analysis is consistent with specific heat data, which show that the pseudogap behavior does not extend into the overdoped regime of $La_{2-x}Sr_xCuO_4$.[28] This is evidence that no gap is observed in the single-particle density of state in the overdoped regime.

VI. CONCLUSION

In this work, we addressed the issue of the optical gap observed in $La_{2-x}Sr_xCuO_4$ (and observed in other HTSC's too). We modeled the CuO_2 layers of this material using a two-dimensional array of double-well potentials in order to explain the origin of this IR optical gap. Each of these double-well potentials reflects on the copper-oxygen-copper unit structure of the CuO_2 layers. Within the tight-binding approach, we assembled these double-well potentials, and a structure with two bands separated by an energy gap is obtained. This is the gap that is used to model the IR optical gap. The doping dependence of this gap, which is deduced from fitting the reflectance data, is found to follow a quadratic law. We argued that the optical gap modeled here is different from the pseudogap or the two-magnon gap observed in $La_{2-x}Sr_xCuO_4$ too. This is because of their different doping dependences, and the fact that the optical gap can be observed even above the pseudogap temperature.[12] The pseudogap seems to vanish near optimal doping whereas the optical gap is nonzero even in the overdoped regime, and remains significant at room temperature close to optimal doping.[26]

According to the present study, if our proposal of the

optical gap being distinct from the pseudogap and two-magnon gap in $La_{2-x}Sr_xCuO_4$ is correct then the analysis of the optical data should be made using a conductivity or dielectric function that results from a system of electrons in two bands with interactions (Coulomb, etc.) giving rise to the pseudogap and the gap between the two bands giving rise to the optical gap. The spin fluctuations on the other hand give rise to the two-magnon gap. We expect that this dielectric function would reflect on the contribution from the optical gap and a generalized Drude term that takes into account a temperature and frequency dependent scattering rate due to the interaction of the electrons with the bosons associated with the spin fluctuations, etc.

Acknowledgments

M.A. would like to acknowledge the financial support from the Natural Science and Engineering Research Council of Canada (NSERC) and the Laurentian University Research Fund (LURF).

[1] M.A. Quijada, D.B. Tanner, R.J. Kelley, M. Onellion, H. Berger, and G. Margaritondo, Phys. Rev. B **60**, 14917 (1999).
[2] S. Uchida, T. Ido, H. Takagi, T. Arima, Y. Tokura, and S. Tajima, Phys. Rev. B **43**, 7942 (1991).
[3] J. Orenstein, G.A. Thomas, D.H. Rapkine, C.G. Bethea, B.F. Levine, R.J. Cava, E.A. Rietman, and D.W. Johnson, Jr., Phys. Rev. B **36**, 729 (1987).
[4] S. Etemad, D.E. Aspnes, M.K. Kelly, R. Thompson, J.-M. Tarascon, and G.W. Hull, Phys. Rev. B **37**, 3396 (1988).
[5] K. Kamaras, S.L. Herr, C.D. Porter, N. Tache, D.B. Tanner, S. Etemad, T. Venkatesan, E. Chase, A. Inam, X.D. Wu, M.S. Hedge, and B. Dutta, Phys. Rev. Lett. **64**, 84 (1990).
[6] A.V. Puchkov, D.N. Basov, and T. Timusk, J. Phys.: Condens. Matter **8**, 10049 (1996).
[7] T. Timusk and B. Statt, Rep. Prog. Phys. **62**, 61 (1999).
[8] F. Marsiglio and J.P. Carbotte, Aust. J. Phys. **50**, 975 (1997)
[9] See S. Hüfner, in *Photoelectron Spectroscopy Principles and Applications*, Chap. 5, Ed. Springer for a discussion of hybridization issue, 2003.
[10] E. Dagotto, Rev. Mod. Phys. **66**, 763 (1994).
[11] J. Labbé and J. Bok, Europhysics Lett. **3**, 1225 (1987).
[12] S. Lupi, P. Calvani, M. Capizzi, and P. Roy, Phys. Rev. B **62**, 12418 (2000).
[13] J.J. Sakurai, *Modern Quantum Mechanics*, Benjamin/Cummings Pub. Co, 1985.
[14] W.A. Harrison, *Solid State Theory*, Dover Publications, New York (1980).
[15] H. Ehrenreich and M.H. Cohen, Phys. Rev. **115**, 786 (1959).
[16] N.W. Ashcroft, N.D. Mermin, in *Solid State Physics*, Brooks/Cole, 1976.
[17] D.J. Griffiths, in *Introduction to electrodynamics*, Prentice Hall, p. 399, 1999.
[18] M. Azzouz, Phys. Rev. B **68**, 174523 (2003).
[19] M. Azzouz, Phys. Rev. B **67**, 134510 (2003).
[20] M. Azzouz, Phys. Rev. B **70**, 052501 (2004).
[21] Y.J. Uemura, G.M. Luke, B.J. Sternlieb, J.H. Brewer, J.F. Carolan, W.N. Hardy, R. Kadono, J.R. Kempton, R.F. Kiefl, S.R. Kreitzman, P. Mulhern, T.M. Riseman, D.Ll. Williams, B.X. Yang, S. Uchida, H. Takagi, J. Gopalakrishnan, A.W. Sleight, M.A. Subramanian, C.L. Chien, M.Z. Cieplak, Gang Xiao, V.Y. Lee, B.W. Statt, C.E. Stronach, W.J. Kossler, and X.H. Yu, Phys. Rev. Lett. **62**, 2317 (1989).
[22] G. Rietveld, N.Y. Chen, and D. van der Marel, Phys. Rev. Lett. **69**, 2578 (1992).
[23] A.G. Loeser, Z.-X. Shen, D.S. Dessau, D.S. Marshall, C.H. Park, and P. Fournier, A. Kapitulnik, Science **273**, 325 (1996).
[24] D.S. Marshall, D.S. Dessau, A.G. Loeser, C-H. Park, A.Y. Matsuura, J.N. Eckstein, I. Bozovic, P. Fournier, A. Kapitulnik, W.E. Spicer, and Z.-X. Shen, Phys. Rev. Lett. **76**, 4841 (1996).
[25] J.L. Tallon and J.W. Loram, Physica C **349**, 53 (2001).
[26] J.G. Naeini, J.C. Irwin, T. Sasagawa, Y. Togawa, and K. Kishio, Can. J. Phys. **78**, 483 (2000).
[27] T. Startseva, T. Timusk, A.V. Puchkov, D.N. Basov, H.A. Mook, M. Okuya, T. Kimura, and K. Kishio, Phys. Rev. B **59**, 7184 (1999).
[28] J.W. Loram, K.A. Mirza, J.R. Cooper, and J.L.Tallon, J. Phys. Chem. Solids, **59**, 2091 (1998).
[29] A. Ino, T. Mizokawa, K. Kobayashi, A. Fujimori, T. Sasagawa, T. Kimura, K. Kishio, K. Tamasaku, H. Eisaki, and S. Uchida, Phys. Rev. Lett. **81**, 2124 (1998).
[30] S. Sugai and T. Hosokawa, Phys. Rev. Lett. **85**, 1112 (2000).
[31] T. Startseva, T. Timusk, M. Okuya, T. Kimura, and K. Kishio, Physica C **321**, 135 (1999).
[32] V.J. Emery and S.A. Kivelson, Nature **374**, 434 (1995).
[33] B. Batlogg, H.Y. Hwang, H. Takagi, R.J. Cava, H.L. Kao, and J. Kuo, Physica C **235/240**, 130 (1994).